nature portfolio

https://doi.org/10.1038/s41565-021-01022-y

Supplementary information

Scalable two-step annealing method for preparing ultra-high-density single-atom catalyst libraries

In the format provided by the authors and unedited

Supplementary information for

Scalable two-step annealing method for preparing ultra-high-density single-atom catalyst libraries

Xiao Hai[1,10], Shibo Xi[2,10], Sharon Mitchell[3,10], Karim Harrath[4,5,10], Haomin Xu[1], Dario Faust Akl[3], Debin Kong[6], Jing Li[1], Zejun Li[1], Tao Sun[1], Huimin Yang[1], Yige Cui[1], Chenliang Su[7], Xiaoxu Zhao[8], Jun Li[4,5*], Javier Pérez-Ramírez[3*] and Jiong Lu[1,9*]*

[1]Department of Chemistry, National University of Singapore, 3 Science Drive 3, Singapore 117543, Singapore.

[2]Institute of Chemical and Engineering Sciences, Agency for Science, Technology and Research, Singapore 627833, Singapore.

[3]Institute for Chemical and Bioengineering, Department of Chemistry and Applied Biosciences, ETH Zurich, Zurich, Switzerland.

[4]Department of Chemistry, Southern University of Science and Technology, Shenzhen 518055, China.

[5]Department of Chemistry and Key Laboratory of Organic Optoelectronics & Molecular Engineering of the Ministry of Education, Tsinghua University, Beijing 100084, China.

[6]CAS Key Laboratory of Nanosystem and Hierarchical Fabrication, CAS Center for Excellence in Nanoscience, National Center for Nanoscience and Technology, Beijing 100190, China.

[7]SZU-NUS Collaborative Center and International Collaborative Laboratory of 2D Materials for Optoelectronic Science & Technology of Ministry of Education, Engineering Technology Research Center for 2D Materials Information Functional Devices and Systems of Guangdong Province, Institute of Microscale Optoelectronics, Shenzhen University, Shenzhen 518060, China.

[8]School of Materials Science and Engineering, Nanyang Technological University, Singapore 639798, Singapore.

[9]Centre for Advanced 2D Materials and Graphene Research Centre, National University of Singapore, Singapore 117546, Singapore.

[10]These authors contributed equally: Xiao Hai, Shibo Xi, Sharon Mitchell, Karim Harrath.

[*]E-mails: xiaoxu.zhao@ntu.edu.sg; junli@tsinghua.edu.cn; jpr@chem.ethz.ch; chmluj@nus.edu.sg

Table of Contents

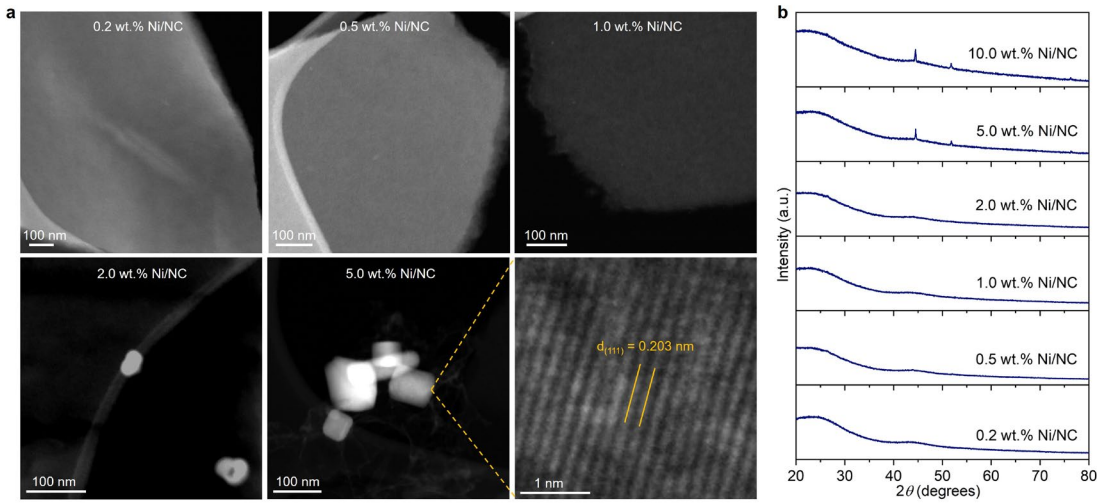

Supplementary Fig. 1 | Catalyst synthesis via one-step annealing. a, b, TEM images (**a**) and XRD patterns (**b**) of Ni/NC catalysts with different metal loadings prepared by impregnation of $NiCl_2$ followed by conventional one-step annealing. The formation of large Ni nanoparticles is readily detected at a metal loading of 2 wt.%, and the particle size gradually increases with higher Ni content. Reflections corresponding to the metallic phase are evident in samples containing 5 and 10 wt.% Ni, and the absence thereof in 2 wt.% Ni/NC suggests that the crystallite sizes are below the detection limit.

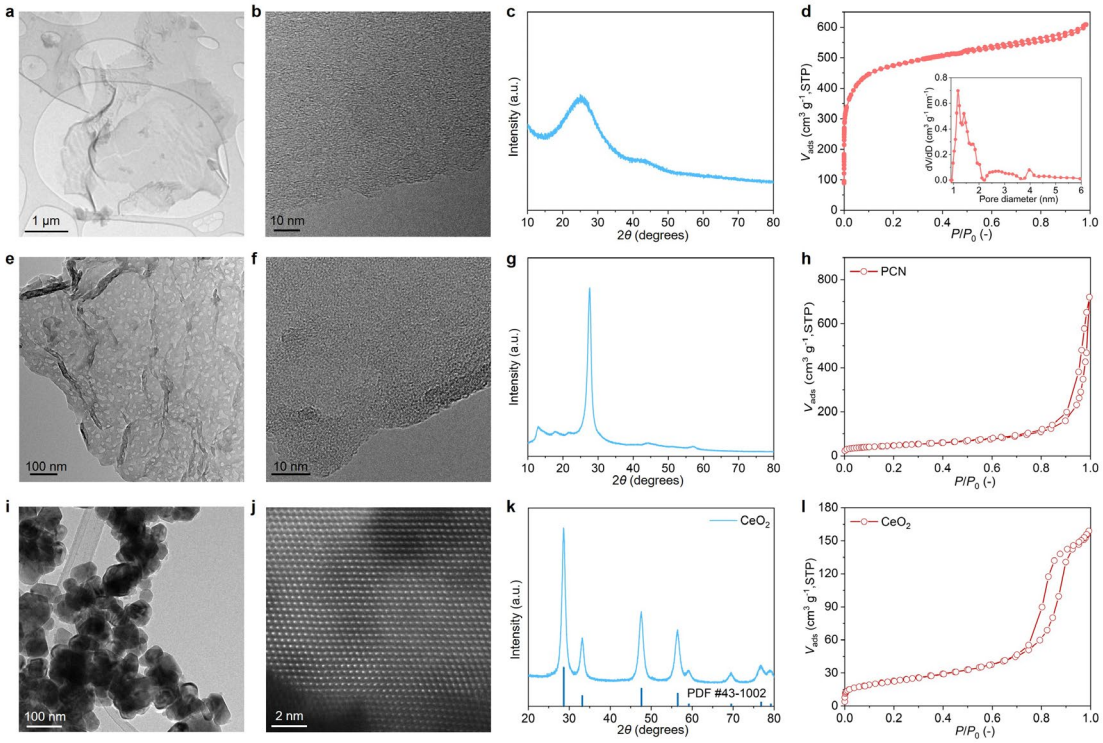

Supplementary Fig. 2 | Characterization of catalyst carriers. Representative low-magnification TEM images of metal-free NC (**a**), PCN (**e**) and CeO_2 (**i**). High-resolution TEM images of NC (**b**), PCN (**f**) and CeO_2 (**j**). XRD patterns of NC (**c**), PCN (**g**) and CeO_2 (**k**). N_2 isotherms of NC (**d**), PCN (**h**) and CeO_2 (**l**). The corresponding derived total surface areas were 1724, 172 and 82 m^2 g^{-1}, respectively.

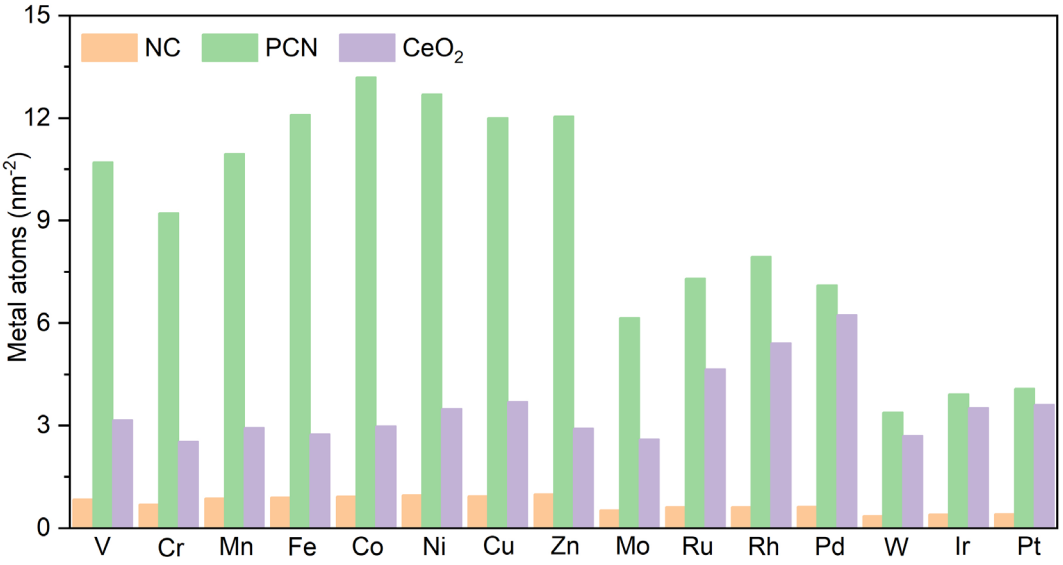

Supplementary Fig. 3 | Surface concentration of metal atoms in UHD-SACs based on NC, PCN, and CeO_2 carriers. The surface concentration was estimated based on the bulk metal content and the specific surface area of the carrier, assuming that all of the metal remains on the carrier surface. Although wet deposition approaches are known to promote surface localization, for certain first row transition metals it may not be the case. For example, Cu and Fe were predicted to percolate preferentially into the bulk of graphitic carbon nitride (*ACS Catal.* **10**, 11069 (2020)), which might explain the significantly higher values observed for PCN compared to NC and CeO_2.

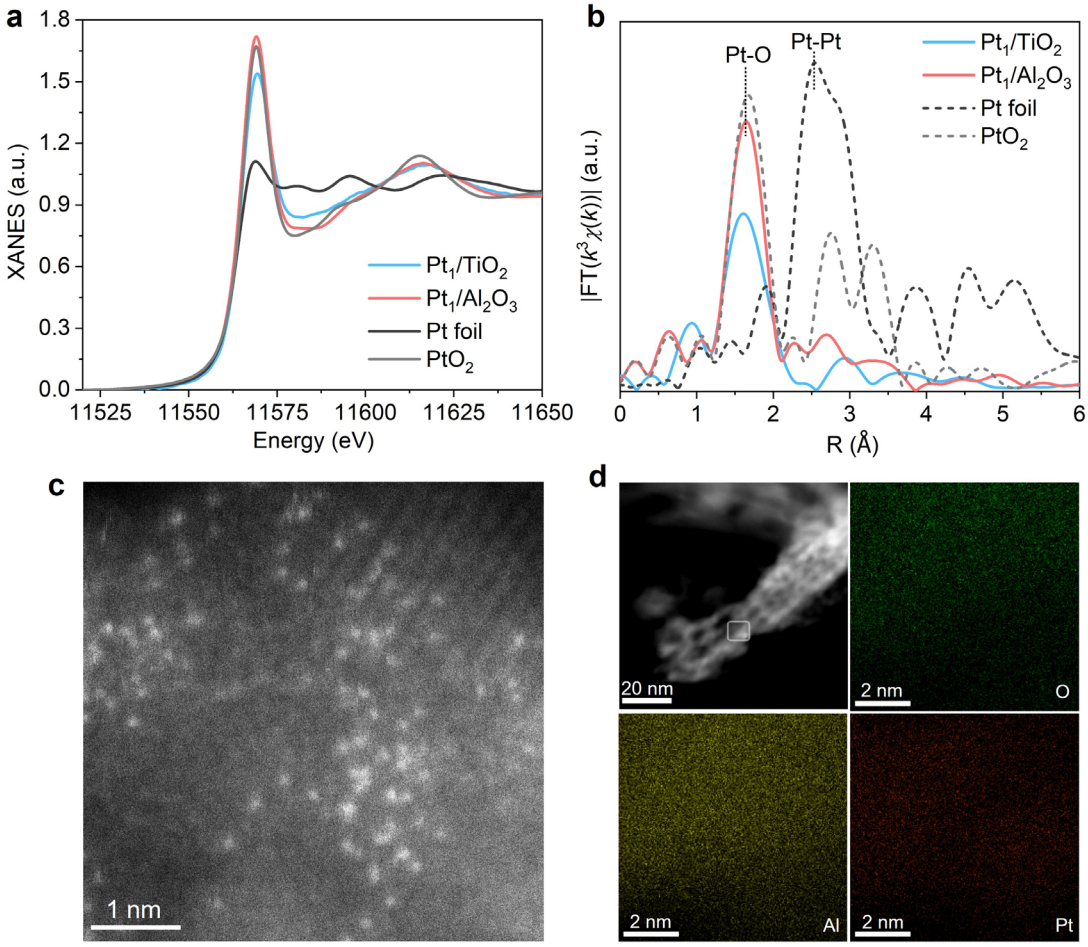

Supplementary Fig. 4 | XANES, EXAFS and STEM characterization of Pt_1/TiO_2 and Pt_1/Al_2O_3 UHD-SACs. The Pt L_3-edge **a**, XANES and **b**, Fourier transformed EXAFS spectra of Pt_1/TiO_2 and Pt_1/Al_2O_3 are compared with Pt references (Pt foil and PtO_2). The intensities of the white line of Pt_1/TiO_2 and Pt_1/Al_2O_3 are close to PtO_2, suggesting that the Pt atoms are positively charged. Besides, the Fourier transformed EXAFS magnitude of Pt_1/TiO_2 and Pt_1/Al_2O_3 are characterized by a single significant peak around 1.63 Å that is close to the location of the Pt-O peak in the PtO_2 reference and thus can be ascribed to Pt-O bonding. The absence of a Pt-Pt peak confirms that Pt species are atomically dispersed on TiO_2 and Al_2O_3. The Pt contents are 8.3 wt.% and 6.8 wt.% for TiO_2 and Al_2O_3, respectively. **c**, Atomic-resolution ADF-STEM image of Pt_1/Al_2O_3 and **d**, corresponding elemental maps of the area indicated.

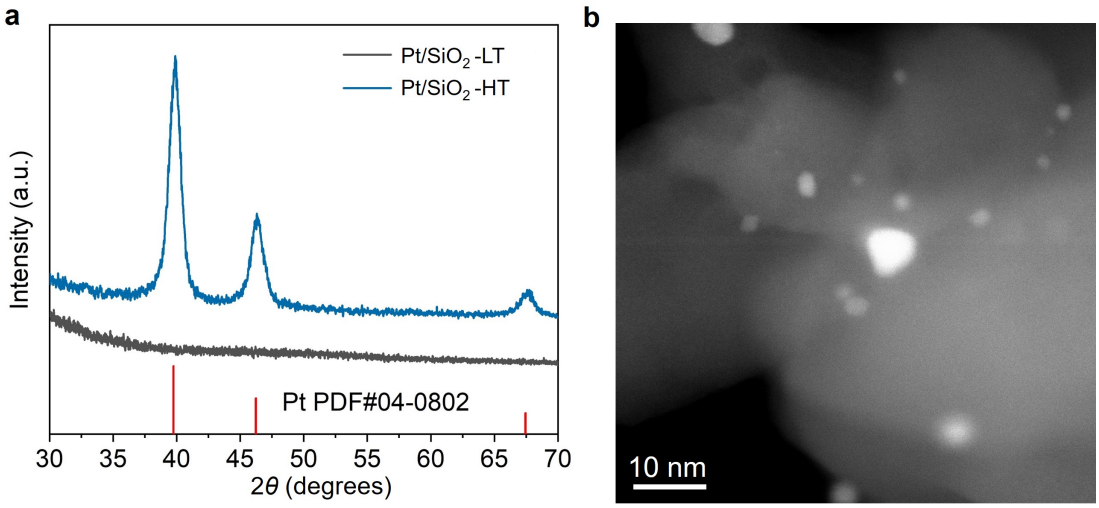

Supplementary Fig. 5 | XRD and TEM characterization of Pt/SiO_2. a, XRD patterns of Pt/SiO_2 after low-temperature (-LT, 200 °C) and high temperature (-HT, 400 °C) annealing. **b**, Dark-field TEM image of Pt/SiO_2-HT. Although surface hydroxyl groups present on silica carriers can act as acids/bases, they are known to be inert and irreducible up to high temperatures. Consistently, Pt single atoms cannot be isolated on amorphous silica with the presented method. Due to the weak bond between surface oxygen and Pt, the atomic dispersion can only be retained up to 200 °C (Pt/SiO_2-LT), above which aggregates are formed (Pt/SiO_2-HT).

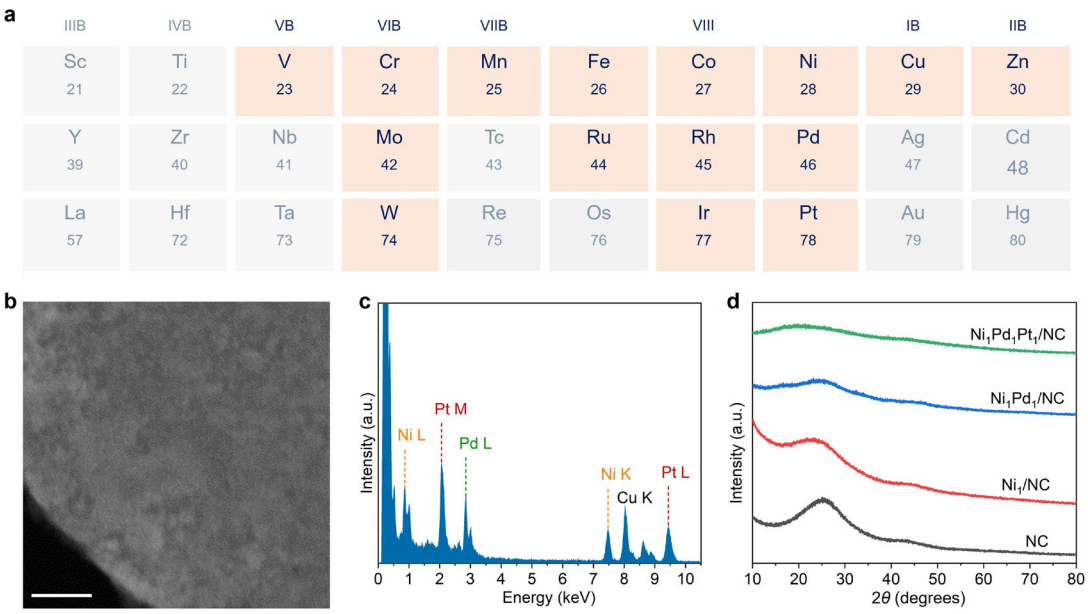

Supplementary Fig. 6 | Multimetallic UHD-SACs. a, Periodic table showing the accessible metals for multimetallic UHD-SACs shaded orange. STEM image (**b**), the corresponding EDS spectra (**c**) of Ni, Pd and Pt in $Ni_1Pd_1Pt_1$/NC. Scale bar: 100 nm. **d**, XRD patterns of Ni_1Pd_1/NC and $Ni_1Pd_1Pt_1$/NC only show the broad reflection at 20-30° and 40-50° belonging to amorphous carbon, no metal-related features can be observed. The Ni and Pd loadings are measured to be 4.2 and 8.6 wt.%, respectively, for Ni_1Pd_1/NC sample. The Ni, Pd and Pt loadings for $Ni_1Pd_1Pt_1$/NC sample were determined as 2.3, 5.1 and 9.8 wt.%, respectively.

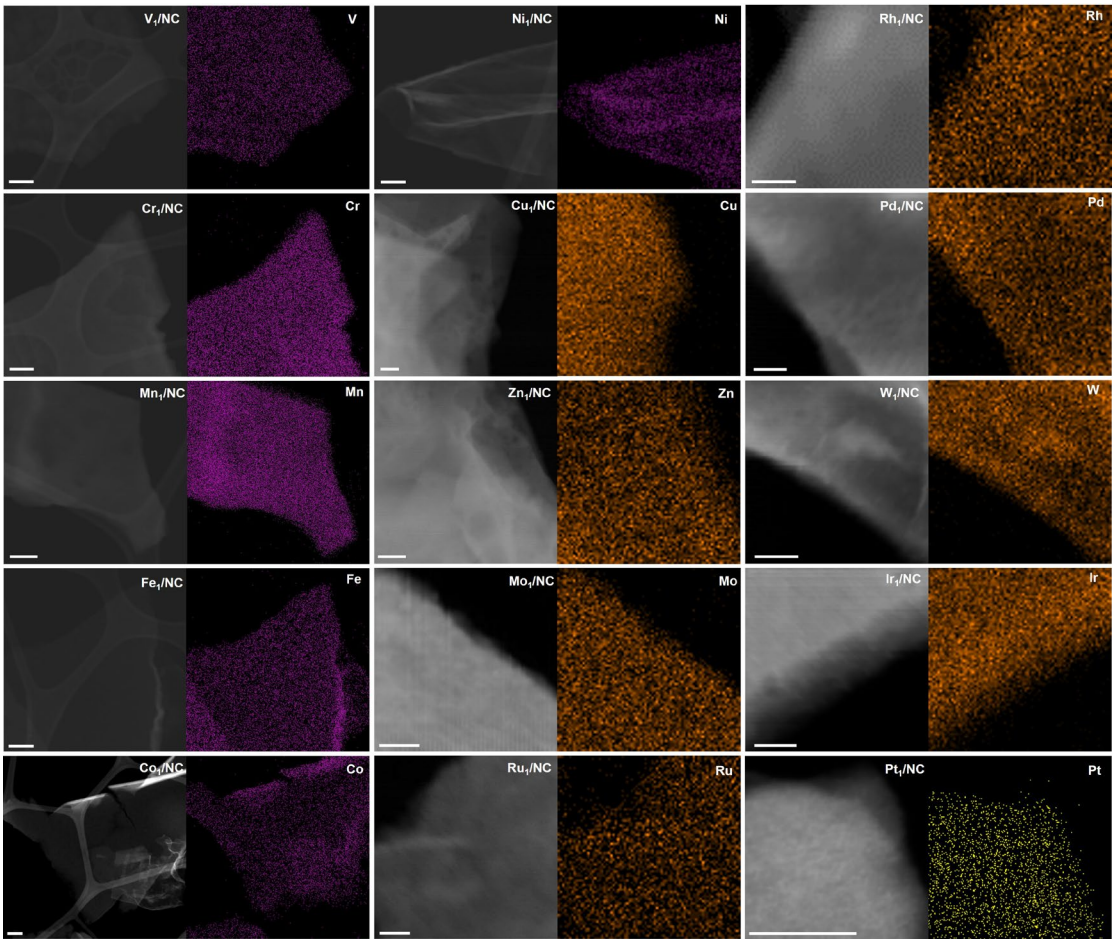

Supplementary Fig. 7 | Elemental mapping of UHD-SACs of various metals on NC. STEM image and corresponding EDS maps of various metals on NC, evidencing the uniform dispersion of metals over the NC support. Scale bars: 100 nm.

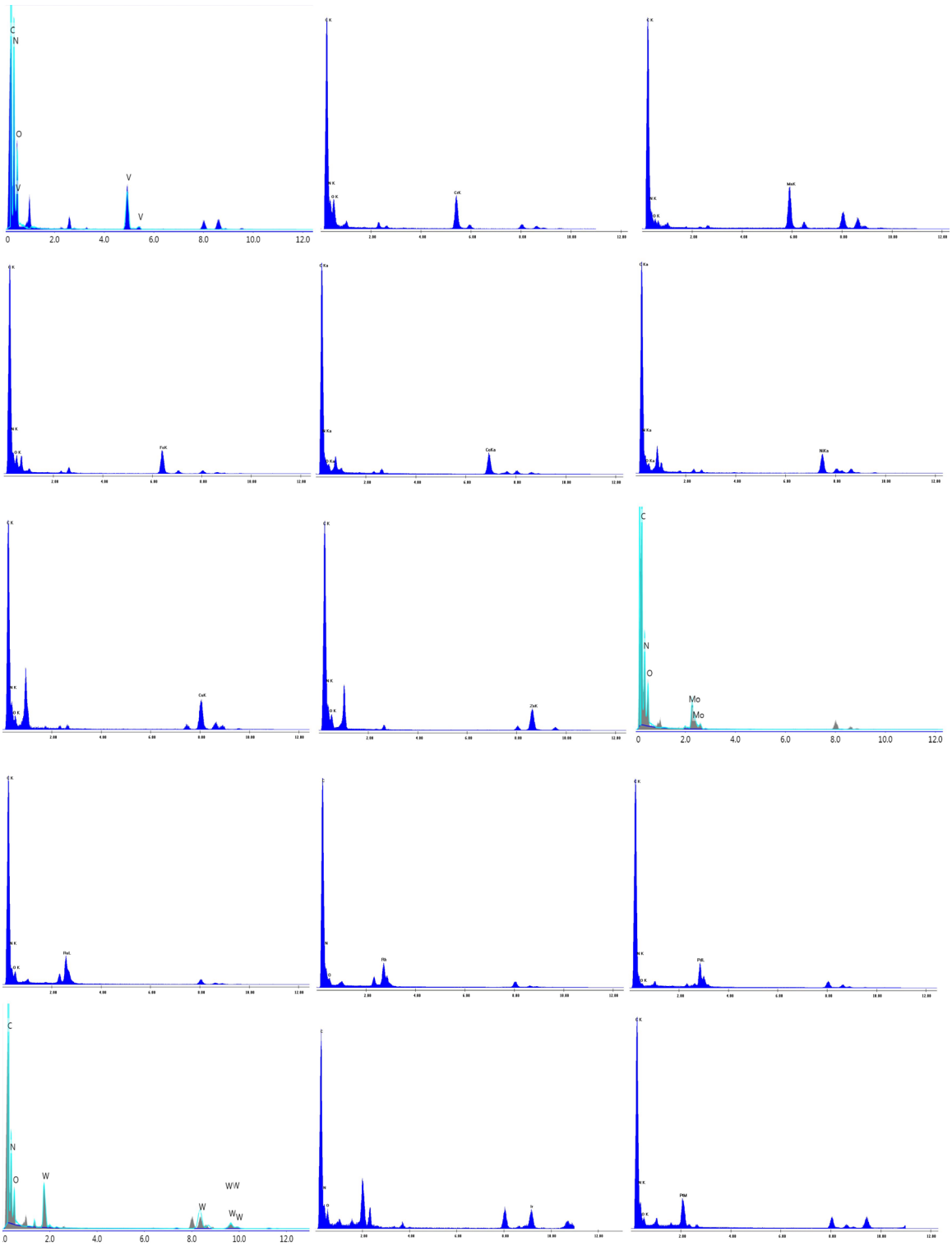

Supplementary Fig. 8 | EDS spectra of various metals on NC support corresponding to the elemental maps presented in **Supplementary Fig. 7**.

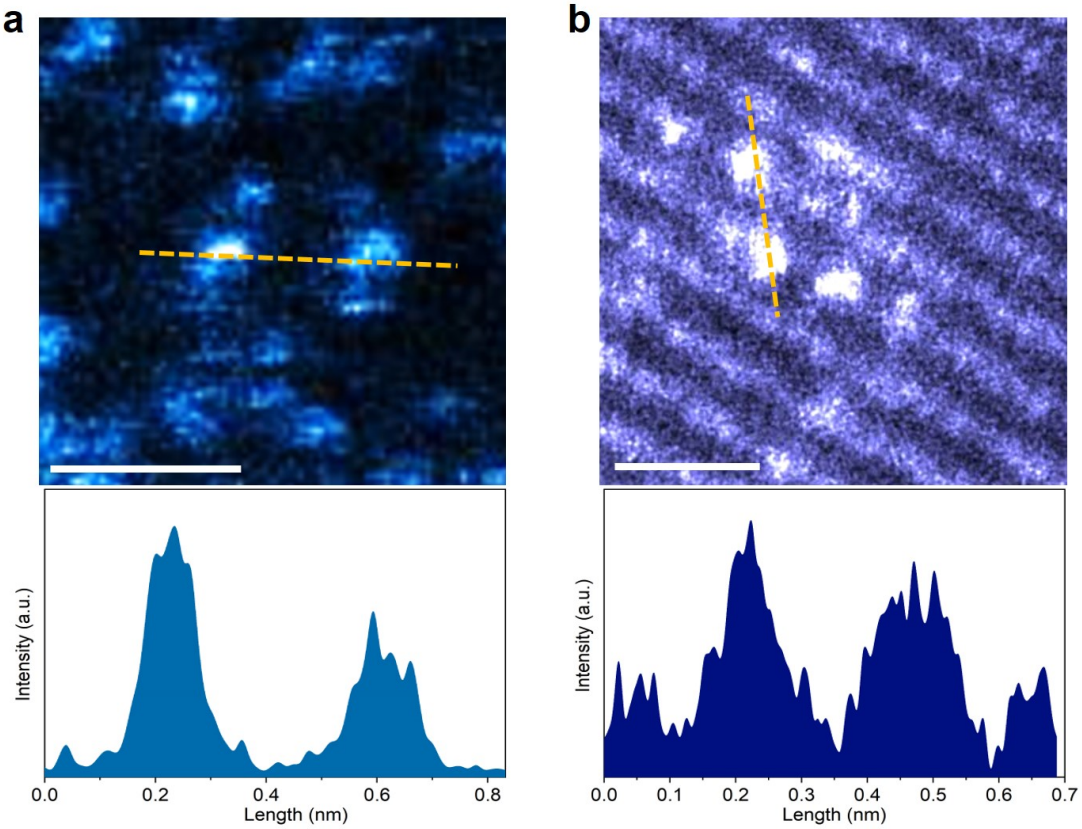

Supplementary Fig. 9 | STEM analysis of Pt_1/PCN and Pt_1/CeO_2. Enlarged areas of the ADF-STEM images of Pt_1/PCN (**a**) and Pt_1/CeO_2 (**b**) line profiles showing the corresponding size of bright dots of approximately 0.2 nm, reflecting the convolution of an isolated Pt atom with the electron probe. Scale bars: 0.5 nm. **c**, STEM image and corresponding EDS maps of Pt_1/CeO_2, evidencing the uniform dispersion of O, Ce and Pt over the support.

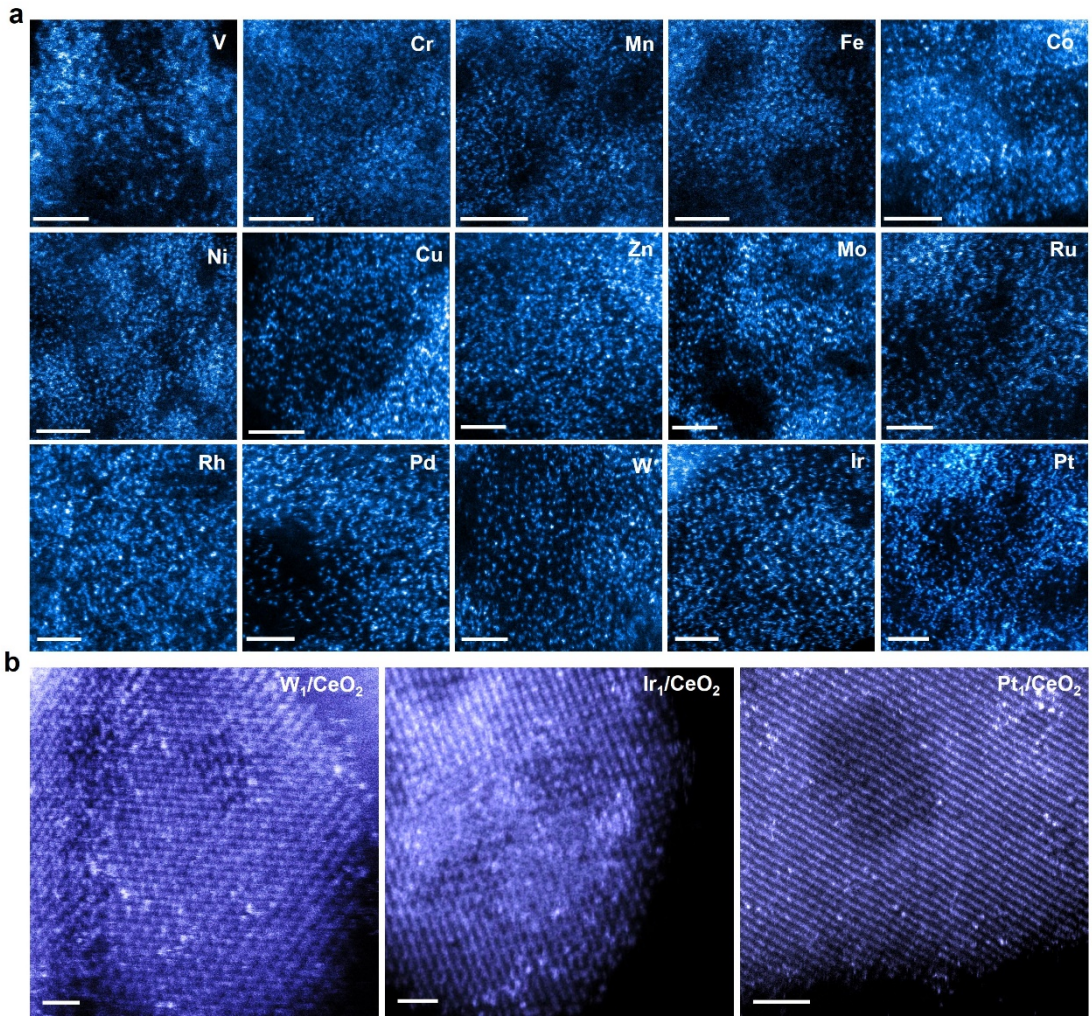

Supplementary Fig. 10 | Visualization of UHD-SACs. Atomic-resolution ADF-STEM images of **a**, various metals on PCN support, **b**, W, Ir and Pt on CeO_2. Scale bars: 1 nm.

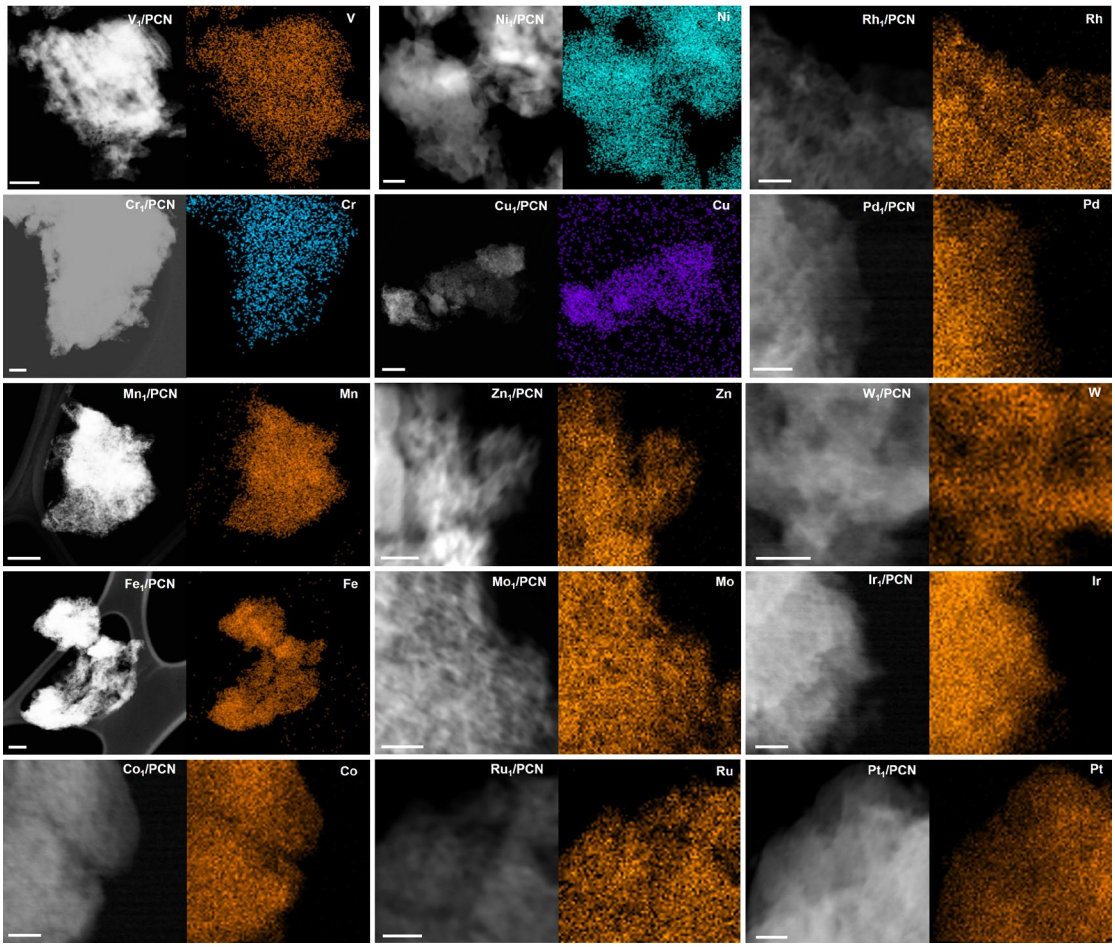

Supplementary Fig. 11 | Elemental mapping of UHD-SACs of various metals on PCN. STEM image and corresponding EDS maps of various metals on PCN, evidencing the uniform dispersion of metals over the support. Scale bars: 100 nm.

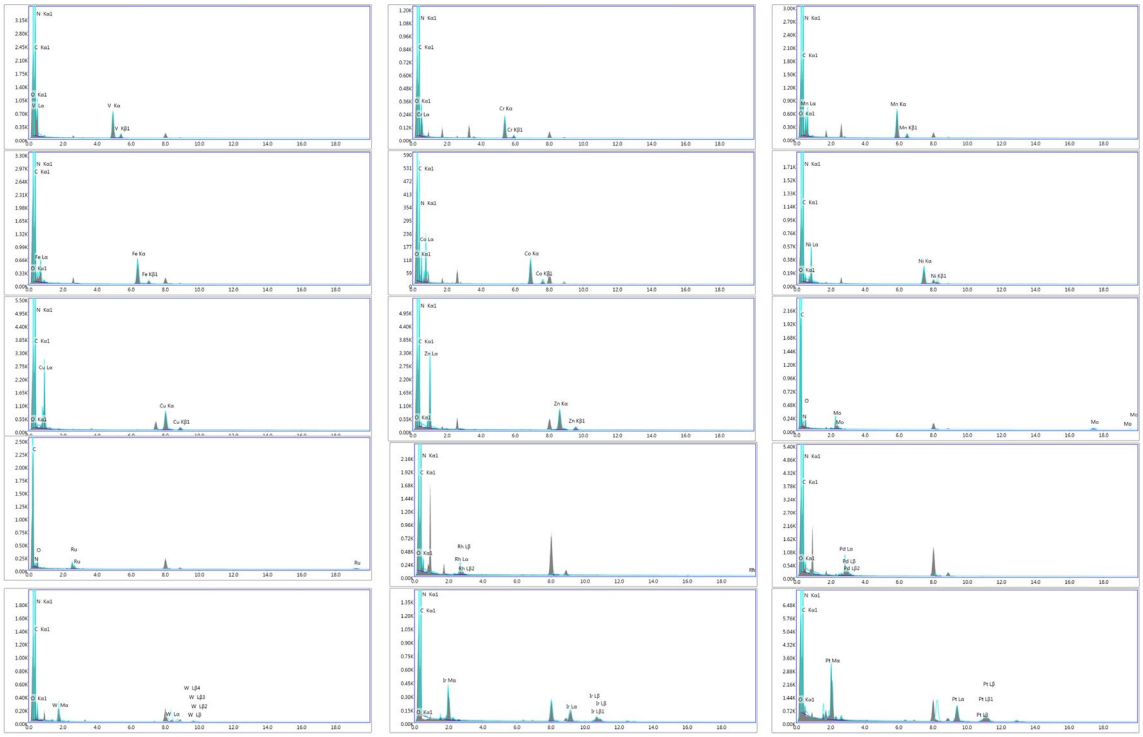

Supplementary Fig. 12 | EDS spectra of various metals on PCN support corresponding to the elemental maps presented in **Supplementary Fig. 11**.

.

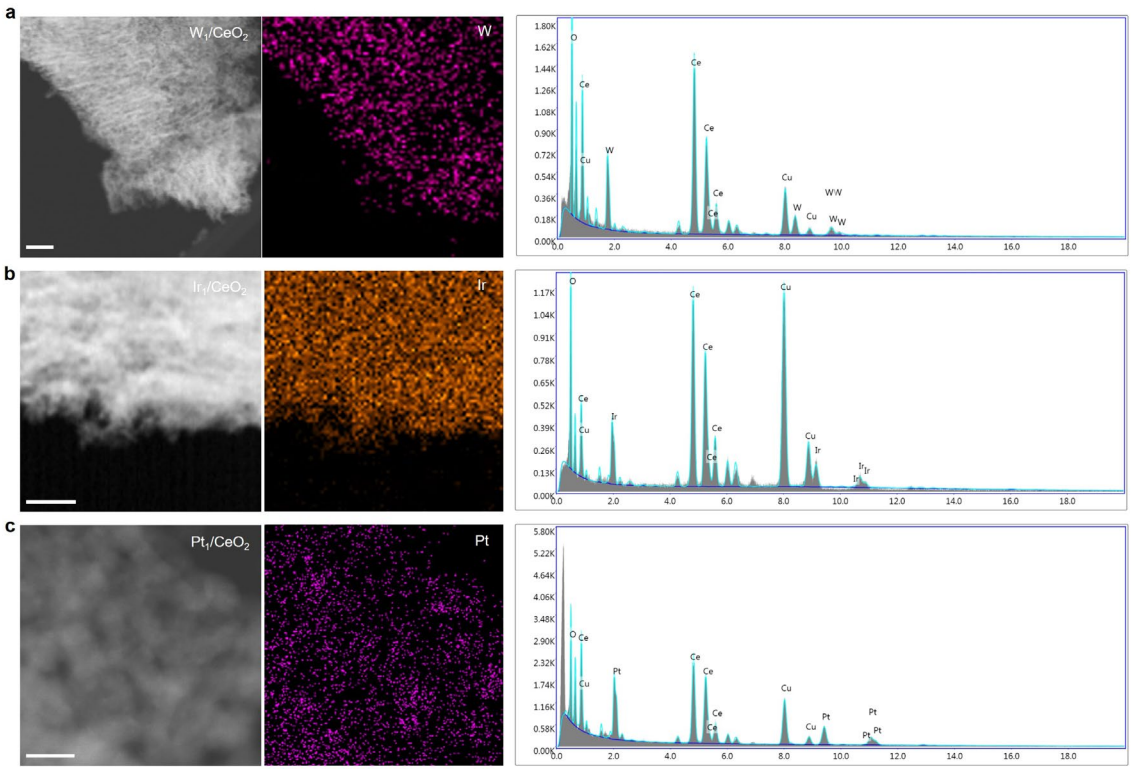

Supplementary Fig. 13 | Elemental mapping of UHD-SACs of W, Ir and Pt on CeO_2. STEM images, corresponding EDS maps and spectra of W, Ir and Pt on CeO_2, evidencing the uniform dispersion of W, Ir and Pt over the support. Scale bars: **a**, **b**, 100 nm; **c**, 10 nm.

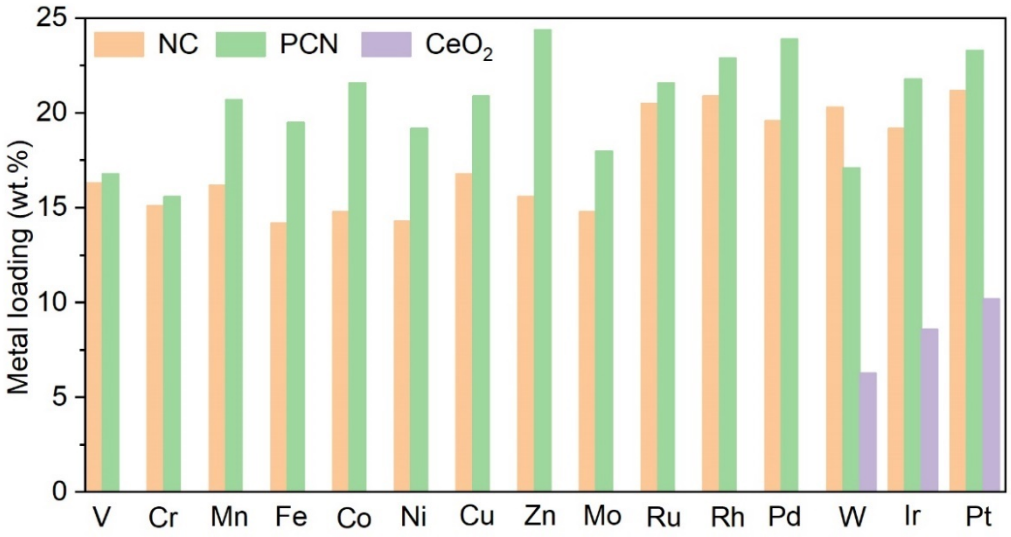

Supplementary Fig. 14 | Metal loadings achieved in this study on NC, PCN, and CeO_2 supports, respectively estimated *via* EDS analysis. The values agree well with the bulk metal contents determined via ICP-OES.

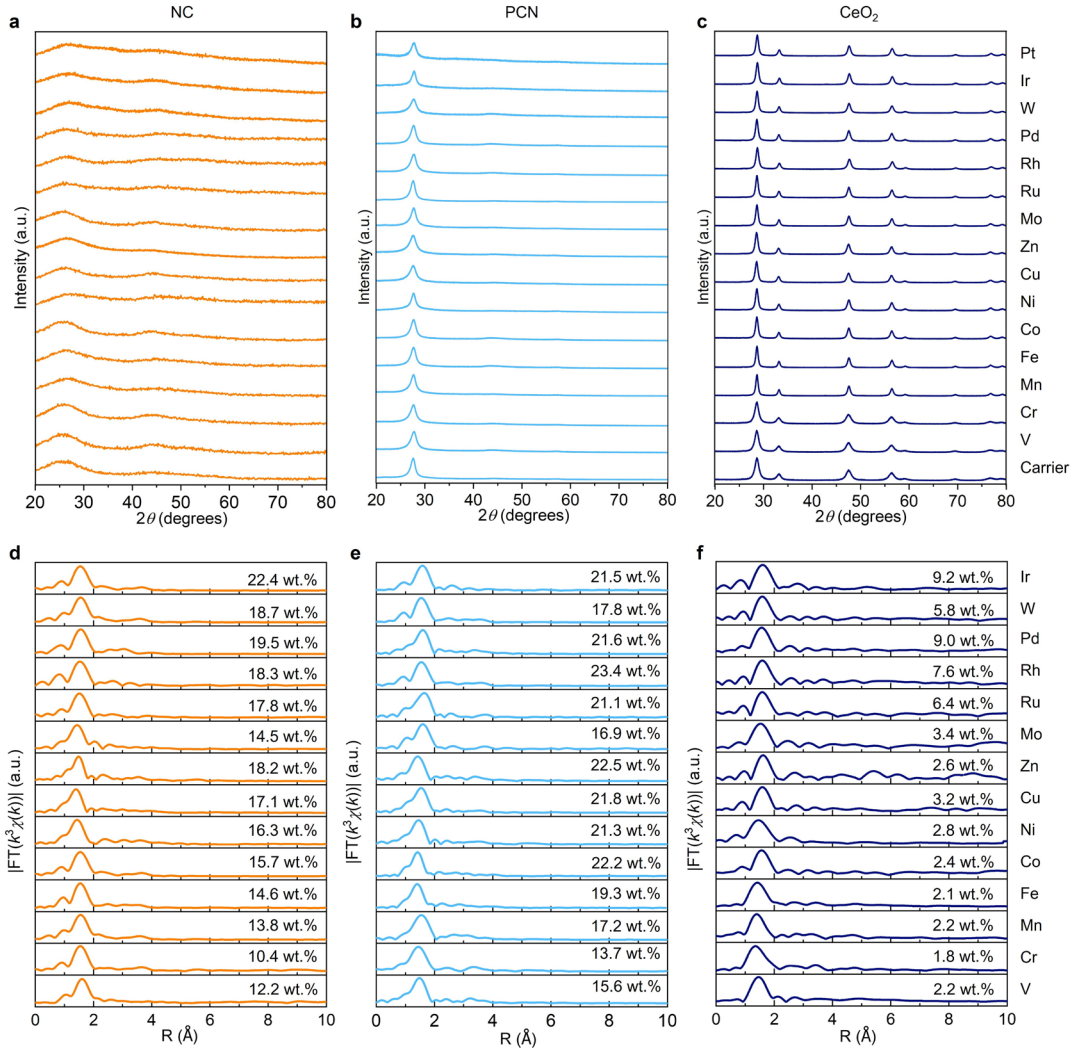

Supplementary Fig. 15 | Additional characterization by XRD and XAS. XRD patterns of UHD-SACs of various metals on **a**, NC, **b**, PCN and **c**, CeO_2. The XRD patterns of all single-atom catalysts only exhibit reflections from the supports, no metal-related signatures can be observed. Fourier transformed EXAFS spectra of UHD-SACs of various metals on NC (**d**), PCN (**e**) and CeO_2 (**f**). The Fourier transformed EXAFS spectra of all single-atom catalysts show the main peak below 2 Å, which can be ascribed to the metal-N/O bonding. No metal-metal bond is detected in any of the samples, confirming the metals are atomically dispersed on the supports.

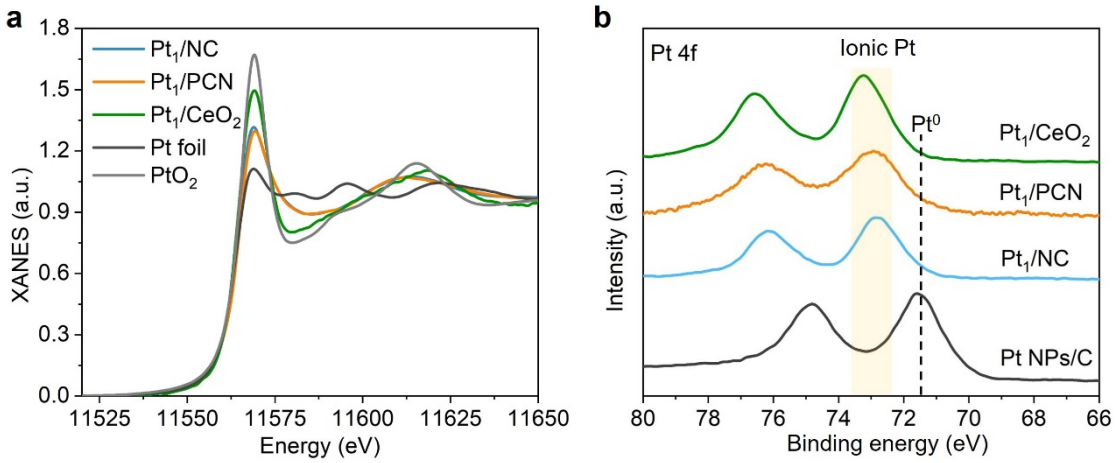

Supplementary Fig. 16 | XPS and XANES analysis of Pt UHD-SACs. a, Pt L_3-edge XANES spectra of Pt_1/NC, Pt_1/PCN and Pt_1/CeO_2. **b**, Pt 4*f* XPS spectra of Pt_1/NC, Pt_1/PCN and Pt_1/CeO_2.

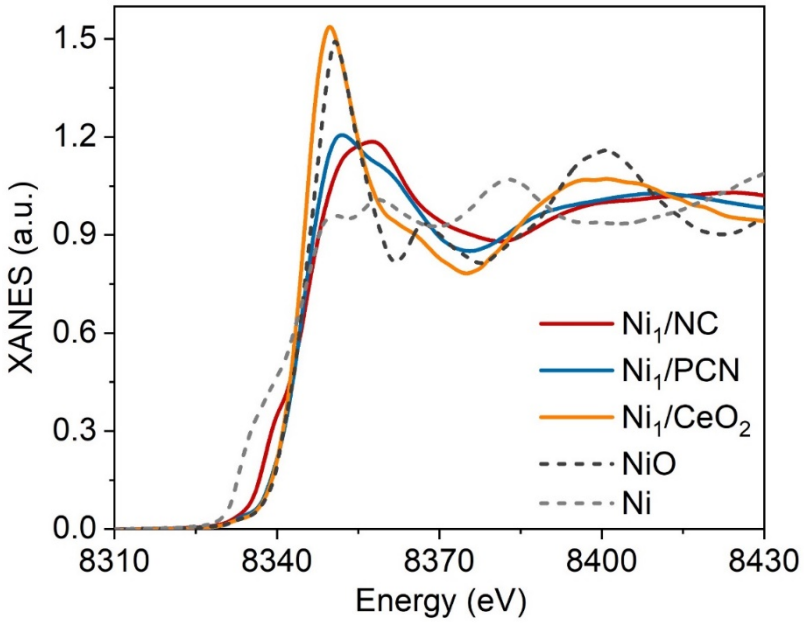

Supplementary Fig. 17 | Ni K-edge XANES spectra of Ni_1/NC, Ni_1/PCN and Ni_1/CeO_2.

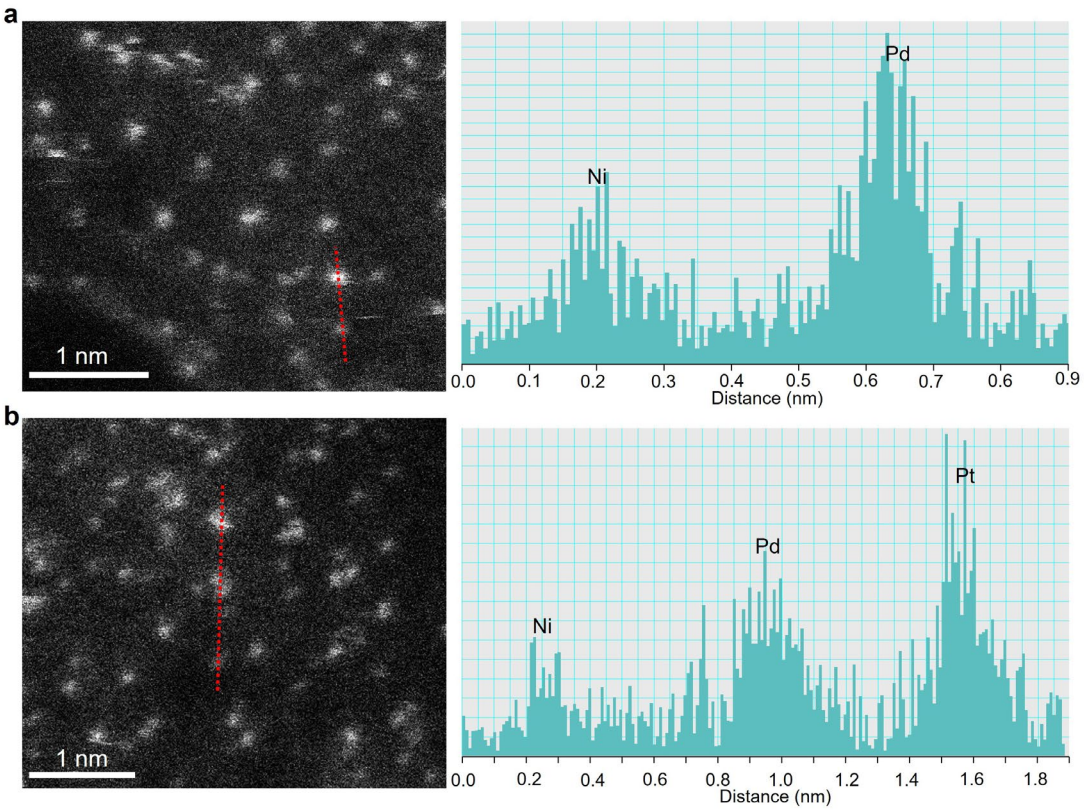

Supplementary Fig. 18 | ADF-STEM images of **a**, Ni_1Pd_1/NC and **b**, $Ni_1Pd_1Pt_1$/NC multimetallic UHD-SACs with corresponding intensity profiles along the dashed red lines.

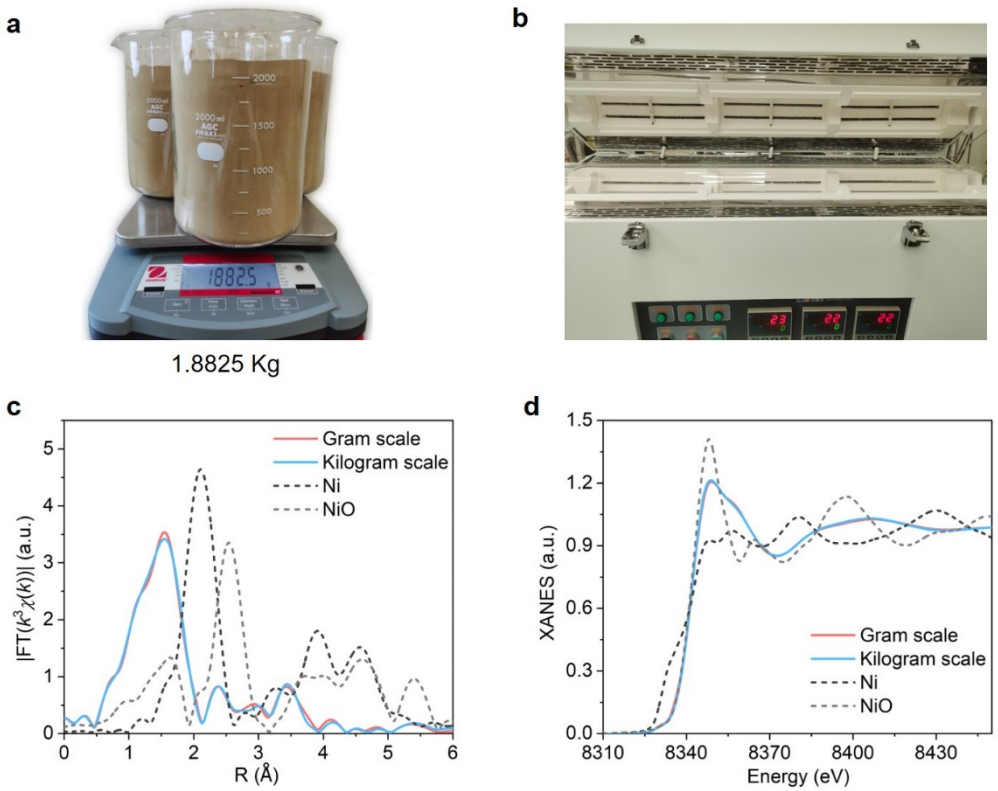

Supplementary Fig. 19 | Production at kilogram scale. Photos of **a**, UHD Ni_1/PCN catalyst synthesized in kilogram scale and **b**, the corresponding tubular furnace used for the synthesis (80 × 1400 mm tube size). Ni K-edge **c**, Fourier transformed EXAFS spectra and **d**, XANES spectra of UHD Ni_1/PCN synthesized at gram and kilogram scales, respectively. The Ni loadings are measured to be 21.3 wt.% and 20.8 wt.% for gram and kilogram scales, respectively.

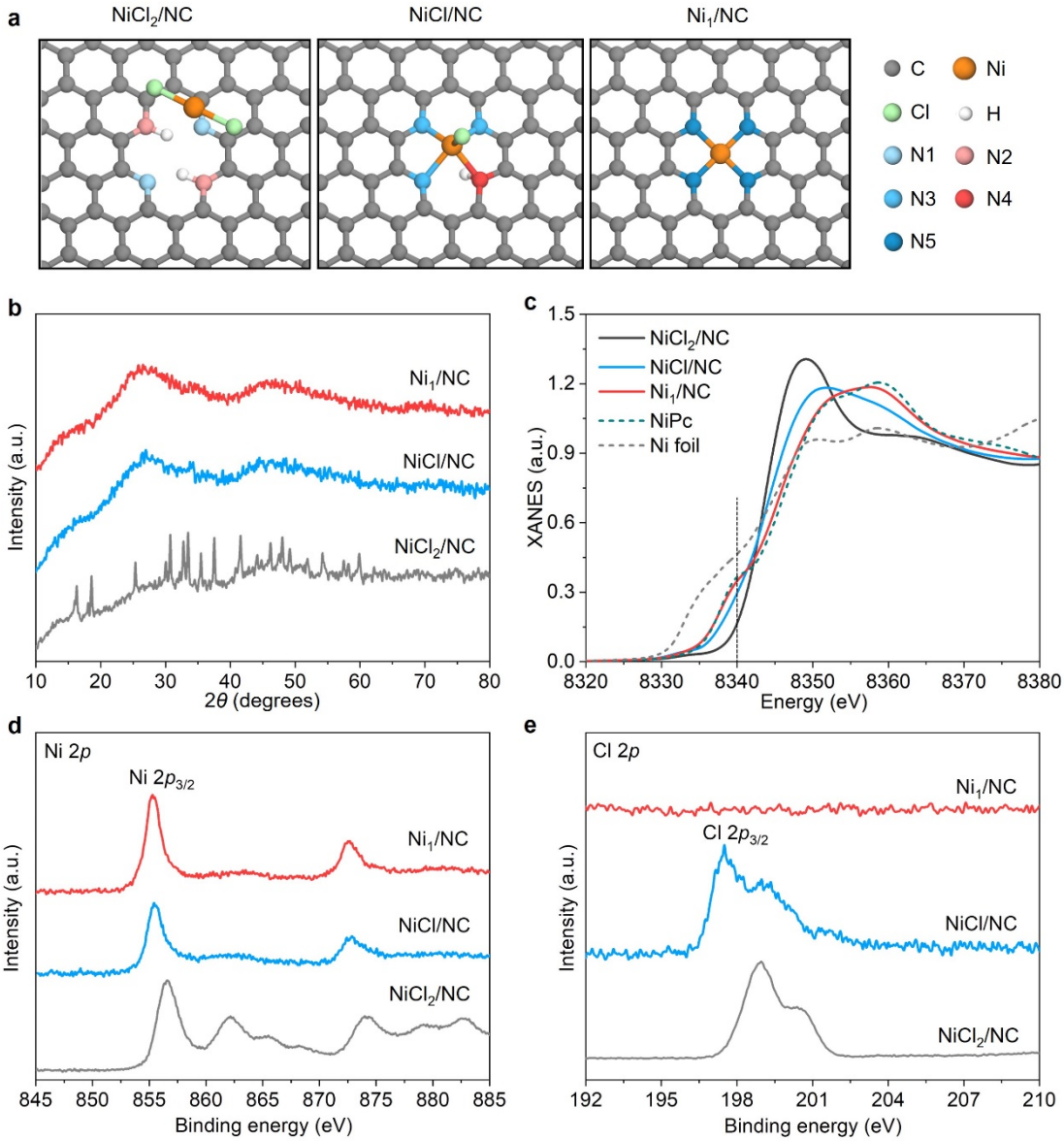

Supplementary Fig. 20 | Structural characterization of $NiCl_2$/NC, NiCl/NC and Ni_1/NC. **a**, Atom-level structural representations of $NiCl_2$/NC, NiCl/NC and Ni_1/NC. **b**, XRD patterns showing the disappearance of reflections arising from $NiCl_2$ after the low-temperature annealing process, indicating that most of the metal precursor reacted with the NC support. **c**, The Ni K-edge XANES spectra of $NiCl_2$/NC, NiCl/NC and Ni_1/NC are compared with NiPc reference. **d**, Ni 2*p* and **e**, Cl 2*p* XPS spectra of $NiCl_2$/NC, NiCl/NC and Ni_1/NC.

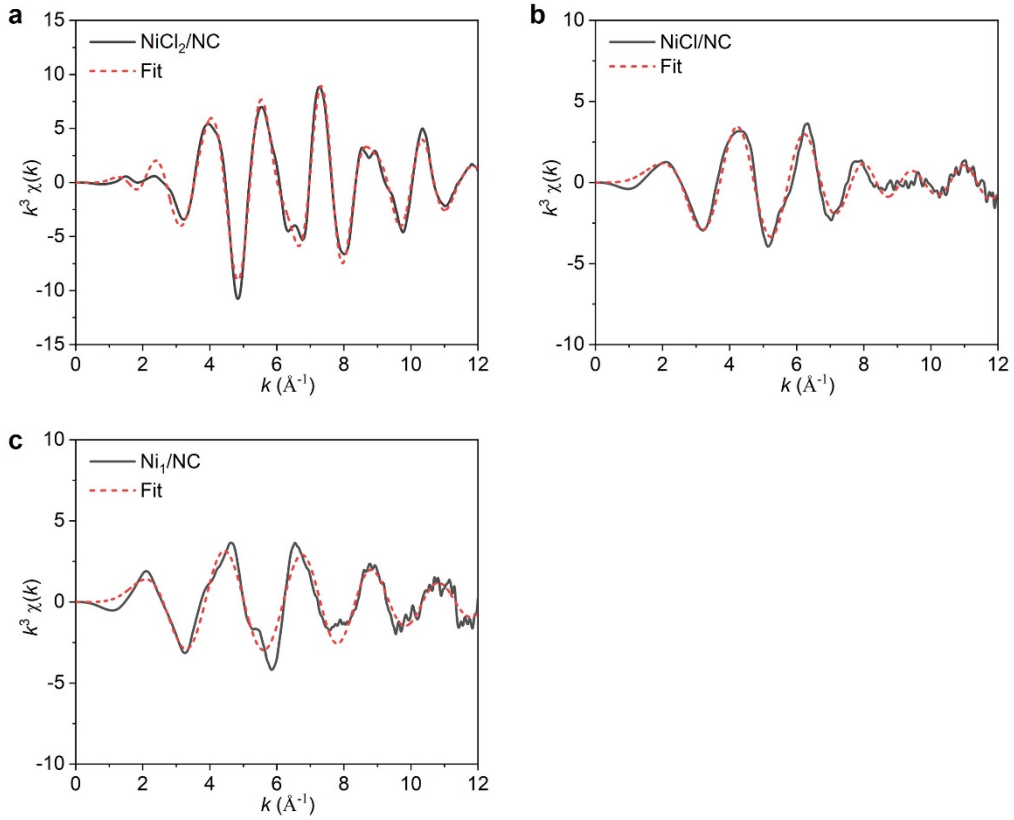

Supplementary Fig. 21 | EXAFS fits of $NiCl_2$/NC, NiCl/NC and Ni_1/NC in *k* plot. EXAFS fits for $NiCl_2$/NC, NiCl/NC and Ni_1/NC evidence a close match between measured and calculated spectra. The fitted parameters are reported in Supplementary **Table 1**.

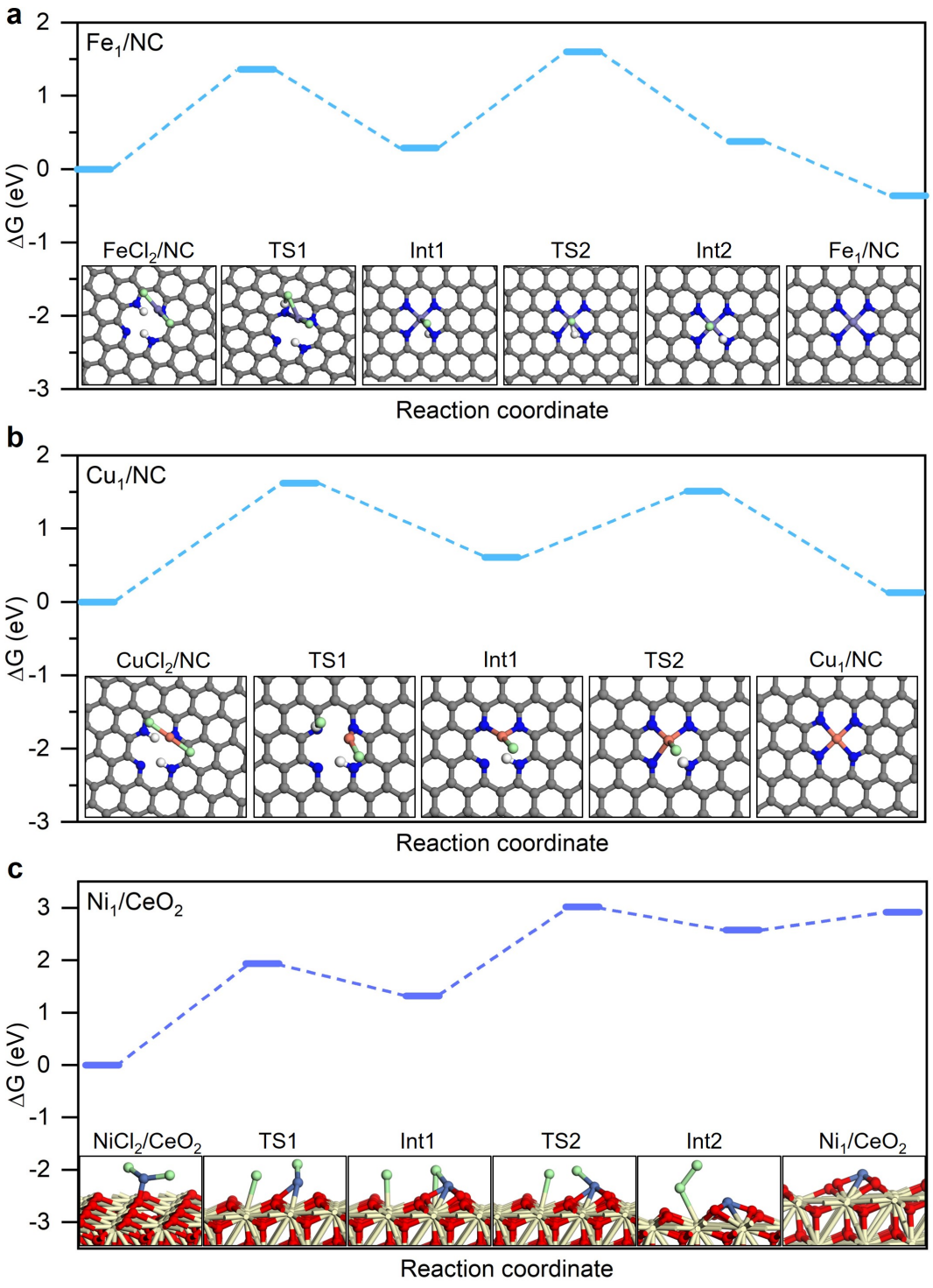

Supplementary Fig. 22 | DFT calculated energy pathways for the formation of **a**, Fe_1/NC, **b**, Cu_1/NC, and **c**, Ni_1/CeO_2 from the respective metal chloride precursors with representative transition states and intermediates depicted inset.

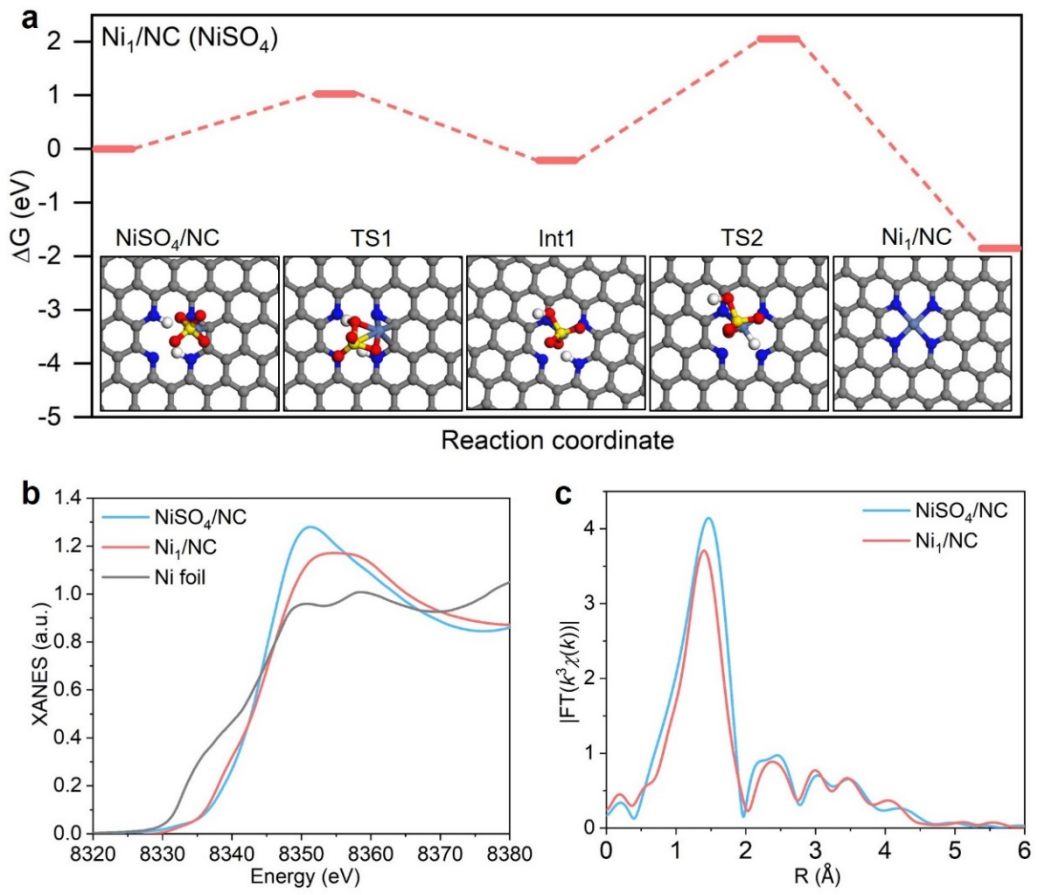

Supplementary Fig. 23 | a, DFT calculated energy pathway for the formation of Ni_1/NC from the $NiSO_4$ precursor with representative transition states and intermediates depicted inset. Ni K-edge **b**, XANES spectra and **c**, Fourier transformed EXAFS spectra of $NiSO_4$/NC and Ni_1/NC. A stepwise removal of the sulphate anion similar to $NiCl_2$ is evidenced. Ni K-edge XANES and Fourier-transformed EXAFS also confirms the presence of the anion in a $NiSO_4$/NC intermediate with broken D_{4h} symmetry, higher valence state and a longer Ni-N bonding length, than the final Ni_1/NC-state. Following the DFT results (**a**), in the first step the anchoring of a single $NiSO_4$ entity to the N4 site in the carrier surmounts a barrier of 1.03 eV. The rotation and abstraction of a hydrogen atom from the carrier (barrier 2.05 eV) is driven by the release of a H_2SO_4 molecule.

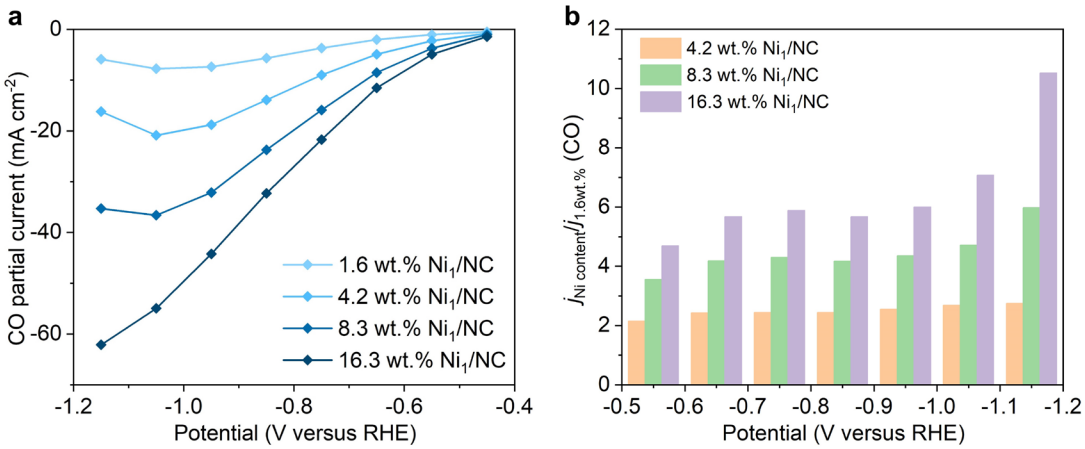

Supplementary Fig. 24 | a, CO partial current density over 1.6 wt.%, 4.2 wt.%, 8.3 wt.% and 16.3 wt.% Ni_1/NC catalysts and **b**, the ratio of CO partial current density to 1.6 wt.% Ni_1/NC catalysts as a function of the potential.

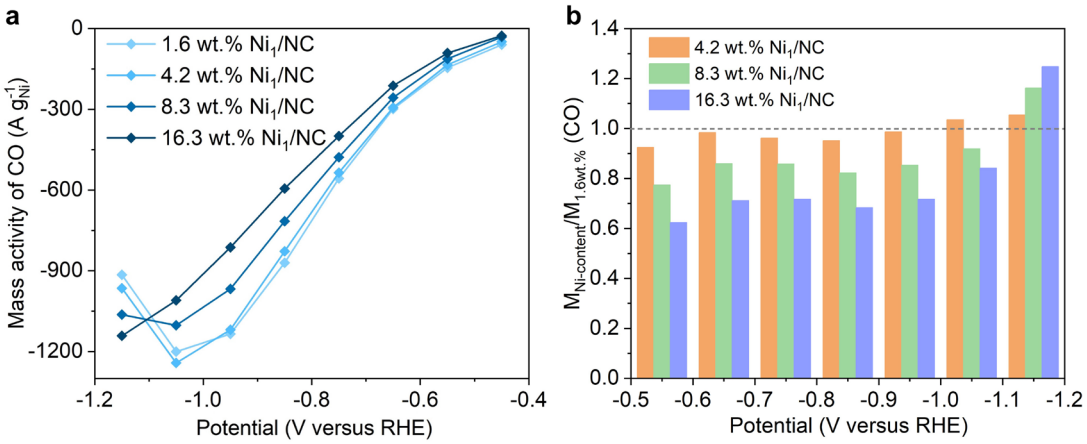

Supplementary Fig. 25 | a, Mass activities of CO over 1.6 wt.%, 4.2 wt.%, 8.3 wt.% and 16.3 wt.% Ni_1/NC catalysts and **b**, the ratio of CO mass activity to 1.6 wt.% Ni_1/NC catalysts as a function of the potential.

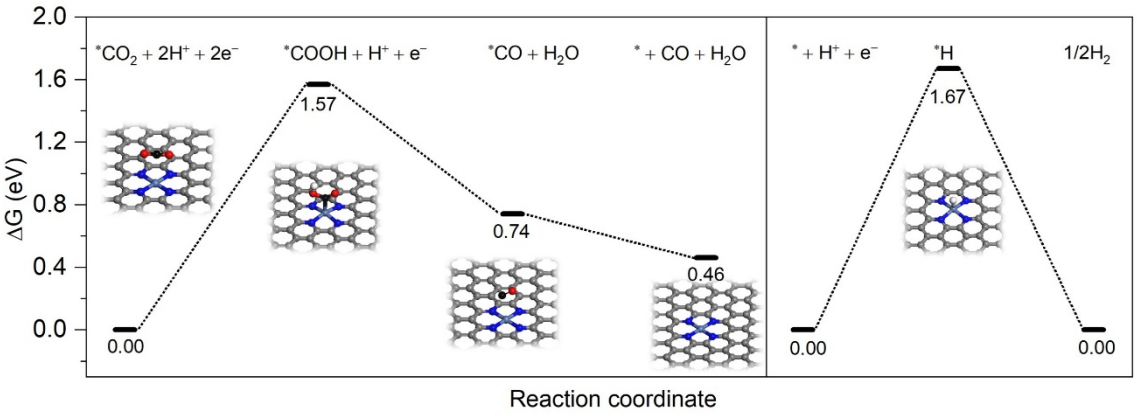

Supplementary Fig. 26 | DFT analysis of the reaction network. DFT calculated binding energy of intermediates on catalysts for the CO_2 reduction (CO2RR) and hydrogen evolution (HER) reactions. A key issue for the electrocatalytic CO_2RR to CO is the rate of the competing HER, where H^+ does not attach to the CO_2 but adsorbs on the catalytic site and then forms a H_2 molecule. Thus, the decisive factor in the selective reduction of CO_2 is the competition between the free energies of *COOH (G_{*COOH}) and *H (G_{*H}) intermediates on each reaction. Our calculations show that G_{*COOH} (1.57 eV) is lower than G_{*H} (1.67 eV). As a result, CO_2RR has lower activation energy than HER, consistent with the high CO_2RR performance observed experimentally.

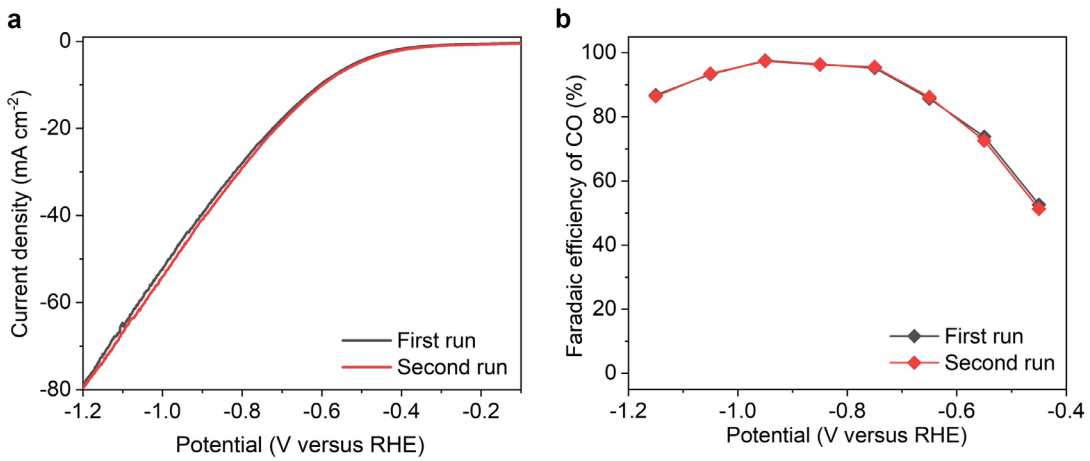

Supplementary Fig. 27 | a, Linear sweep voltammetry curve **b**, Faradic efficiency over 16.3 wt.% Ni_1/NC catalysts for the first and second runs.

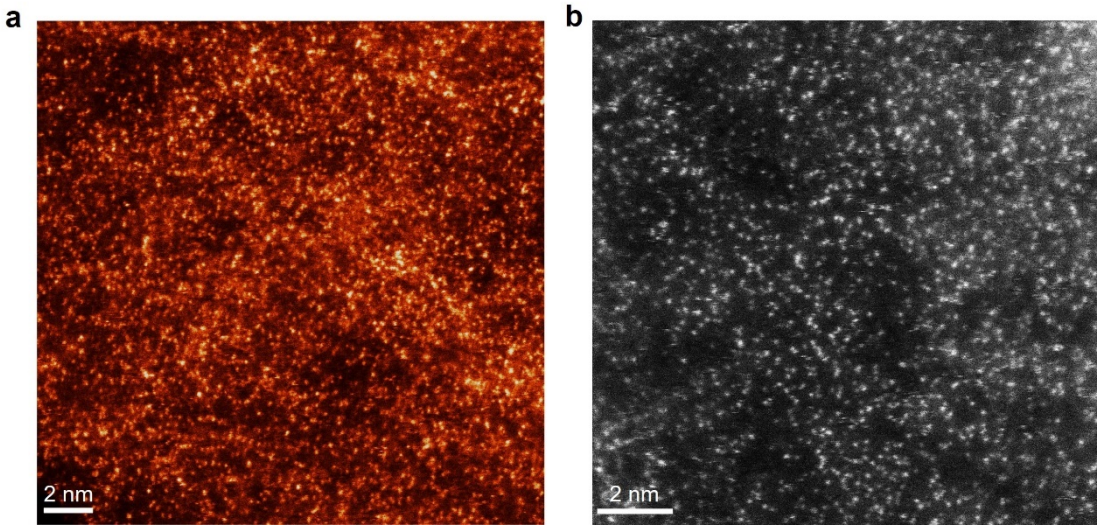

Supplementary Fig. 28 | Atomic-resolution ADF-STEM image of the Ni_1/NC catalyst **a**, before and **b**, after use in the CO_2 reduction reaction.

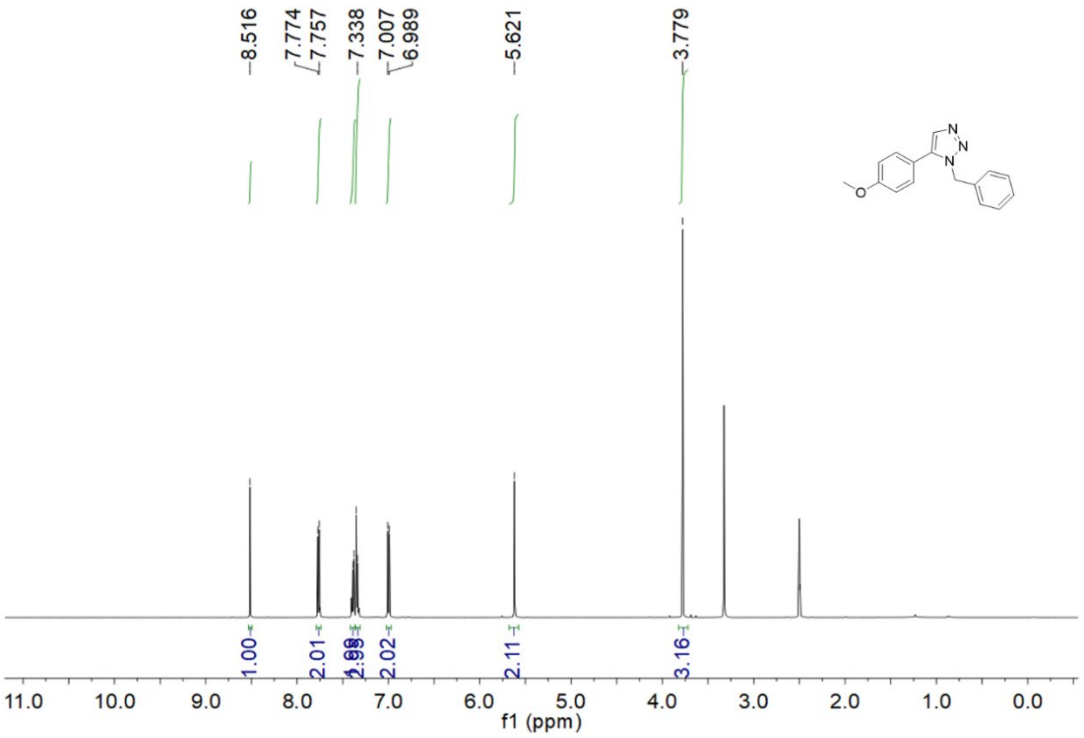

^{1}H NMR (DMSO-*d6*) *δ* [ppm] 8.52 (s, 1H), 7.78 – 7.75 (m, 2H), 7.39 – 7.37 (m, 2H), 7.35 – 7.33 (m, 3H), 7.01 – 6.98 (m, 2H), 5.62 (s, 2H), 3.78 (s, 3H)

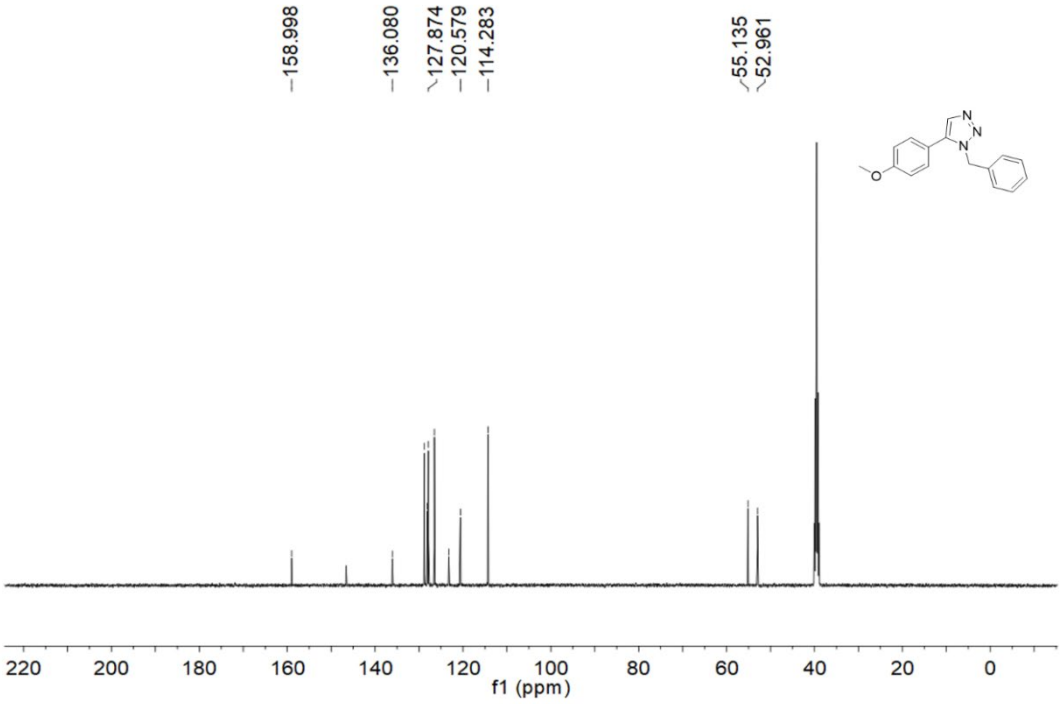

^{13}C NMR (DMSO-*d6*) δ [ppm] 159.0, 136.1, 128.8, 128.1, 127.9, 126.5, 123.3, 120.6, 114.3, 55.1, 53.0.

Supplementary Fig. 29 | ^{1}H and ^{13}C NMR assay for 1-benzyl-5-(4-methoxyphenyl)-1H-1,2,3-triazole.

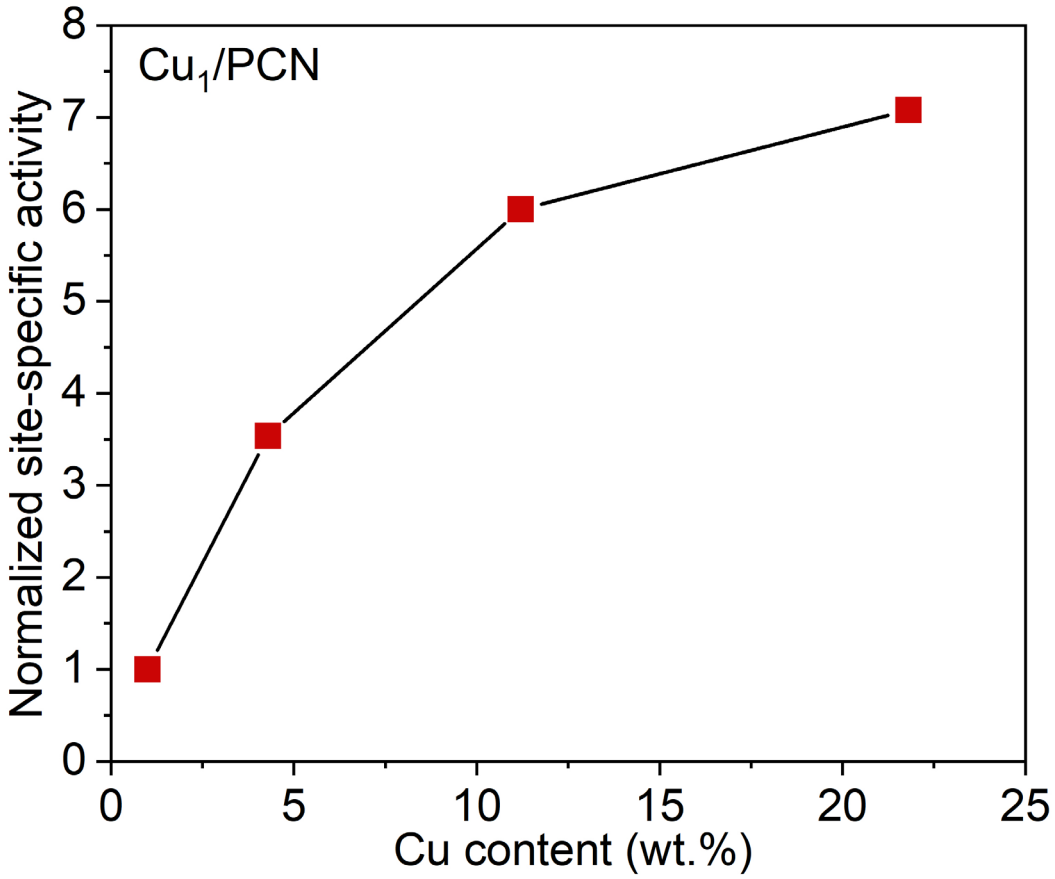

Supplementary Fig. 30 | Normalized site-specific activity of Cu_1/PCN catalysed azide-alkyne cycloaddition of 4-ethynylanisol with benzyl azide to 1.0 wt.% Cu_1/PCN.

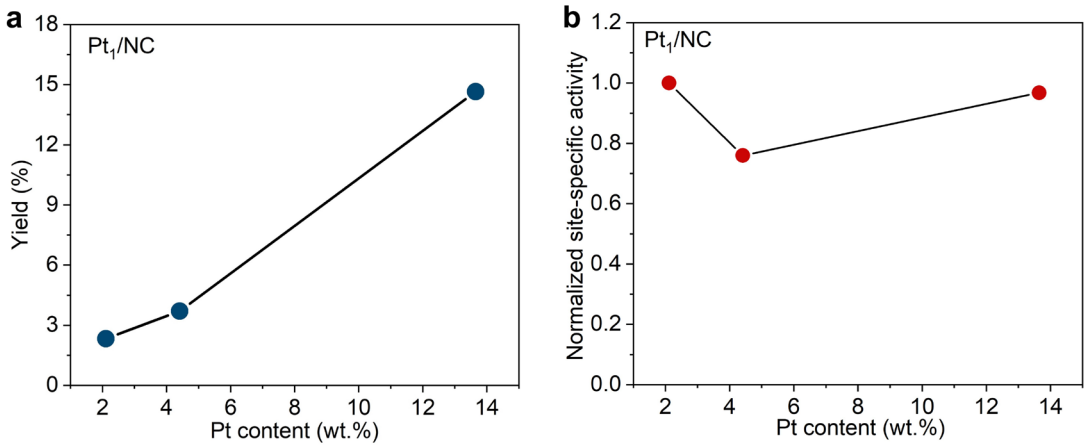

Supplementary Fig. 31 | Pt_1/NC catalysed acetylene hydrochlorination. a, Loading dependent on catalytic performance. **b**, Normalized site-specific activity to 2.1 wt.% Pt_1/NC.

Supplementary Table 1 | Optimization of T_1 in the synthesis of Ni_1/NC using distinct Ni precursors.

Ni precursor	T_1 (°C)[a]	T_2 (°C)	Ni content (wt.%)
$Ni_2(CH_3COO)_2{\cdot}4H_2O$	100	550	4.2
$NiSO_4{\cdot}7H_2O$	300	550	14.4
$NiCl_2{\cdot}6H_2O$	100	550	3.6
$NiCl_2{\cdot}6H_2O$	200	550	9.2
$NiCl_2{\cdot}6H_2O$	300	550	16.3

[a] T_1 is selected to be close to the temperature of decomposition of the Ni precursor. If T_1 is selected to be higher than the temperature of decomposition, then nanoparticle formation is observed. If T_1 is much lower than the decomposition temperature this leads to lower metal contents in the resulting SACs.

Supplementary Table 2 | Results of EXAFS fits of $NiCl_2$/NC, NiCl/NC and Ni_1/NC.

Sample	Shell	*N*	*R* (Å)	σ^2 (10^{-3}Å^2)	R factor
$NiCl_2$/NC	Ni-Cl	6	2.39	0.0076	0.003
	Ni-Ni	6	3.49	0.0145	
NiCl/NC	Ni-N	4.8	1.97	0.0111	0.003
	Ni-Cl	0.9	2.26	0.0032	
Ni_1/NC	Ni-N	4.6	1.89	0.0066	0.013

N, coordination number; *R*, distance between absorbing and backscattering atoms; σ^2, Debye-Waller factor to account for thermal and structural disorders; R factor as a measure of the goodness of fit. The fitted coordination environment of $NiCl_2$/NC, NiCl/NC and Ni_1/NC coincides well with the proposed initial, intermediate and final structures from DFT. For the initial $NiCl_2$/NC, Ni is coordinated to 6 Cl. For the intermediate NiCl/NC, Ni is coordinated to 4 N and 1 Cl. For the final Ni_1/NC, Ni is coordinated to 4 N.

Supplementary Table 3 | Overview of the synthesis conditions used to obtain the UHD-SACs reported in this work. All solutions are based on deionized water unless otherwise specified. Water-ethanol mixtures (H_2O-EtOH) are equivolumetric.

NC substrate

Metal	Metal precursor	Dispersion solvent	T_1 (°C)	Washing solvent	T_2 (°C)
V	VCl_3	EtOH	300	EtOH	550
Cr	CrO_3	H_2O	300	1 M NaOH	550
Mn	$MnCl_2{\cdot}2H_2O$	EtOH	300	H_2O-EtOH	550
Fe	$FeCl_2{\cdot}4H_2O$	EtOH	300	H_2O-EtOH	550
Co	$CoCl_2{\cdot}6H_2O$	EtOH	300	H_2O-EtOH	550
Ni	$NiCl_2{\cdot}6H_2O$	EtOH	300	H_2O-EtOH	550
Cu	$CuCl_2$	EtOH	300	EtOH	500
Zn	$ZnCl_2{\cdot}4H_2O$	EtOH	300	EtOH	550
Mo	$MoCl_5$	EtOH	300	1 M NH_4OH	550
Ru	$RuCl_3{\cdot}xH_2O$	H_2O	300	H_2O	550
Rh	$(NH_4)_3RhCl_6$	H_2O	300	DMSO	550
Pd	$PdCl_2$	0.5 M HCl	200	DMSO or 1 M NH_4OH	550
W	WCl_5	EtOH	300	1 M NH_4OH	550
Ir	$IrCl_3{\cdot}xH_2O$	H_2O	200	DMSO	550
Pt	$H_2PtCl_6{\cdot}6H_2O$	H_2O	200	DMSO or 1 M NH_4Cl	550

PCN substrate

Metal	Metal precursor	Dispersion solvent	T_1 (°C)	Washing solvent	T_2 (°C)
V	VCl_3	EtOH	300	EtOH	500

Cr	CrO_3	H_2O	300	1 M NaOH	500
Mn	$MnCl_2{\cdot}2H_2O$	EtOH	450	H_2O-EtOH	500
Fe	$FeCl_2{\cdot}4H_2O$	EtOH	300	H_2O-EtOH	500
Co	$CoCl_2{\cdot}6H_2O$	EtOH	450	H_2O-EtOH	500
Ni	$NiCl_2{\cdot}6H_2O$	EtOH	450	H_2O-EtOH	500
Cu	$CuCl_2$	EtOH	300	EtOH	500
Zn	$ZnCl_2{\cdot}4H_2O$	EtOH	400	EtOH	500
Mo	$MoCl_5$	EtOH	350	1 M NH_4OH	500
Ru	$RuCl_3{\cdot}xH_2O$	H_2O	300	H_2O	500
Rh	$(NH_4)_3RhCl_6$	H_2O	300	DMSO	500
Pd	$PdCl_2$	0.5 M HCl	300	DMSO or 1 M NH_4OH	500
W	WCl_5	EtOH	350	1 M NH_4OH	500
Ir	$IrCl_3{\cdot}xH_2O$	H_2O	300	DMSO	500
Pt	$H_2PtCl_6{\cdot}6H_2O$	H_2O	300	DMSO or 1 M NH_4Cl	500

CeO_2 substrate

Metal	Metal precursor	Dispersion solvent	T_1 (°C)	Washing solvent	T_2 (°C)
V	VCl_3	EtOH	300	EtOH	500
Cr	CrO_3	H_2O	300	1 M NaOH	500
Mn	$MnCl_2{\cdot}2H_2O$	EtOH	300	H_2O-EtOH	500
Fe	$FeCl_2{\cdot}4H_2O$	EtOH	300	H_2O-EtOH	500
Co	$CoCl_2{\cdot}6H_2O$	EtOH	300	H_2O-EtOH	500
Ni	$NiCl_2{\cdot}6H_2O$	EtOH	300	H_2O-EtOH	500
Cu	$CuCl_2$	EtOH	300	EtOH	500
Zn	$ZnCl_2{\cdot}4H_2O$	EtOH	300	EtOH	500
Mo	$MoCl_5$	EtOH	300	1 M NH_4OH	500
Ru	$RuCl_3{\cdot}xH_2O$	H_2O	300	H_2O	500
Rh	$(NH_4)_3RhCl_6$	H_2O	300	DMSO	500
Pd	$PdCl_2$	0.5 M HCl	300	DMSO or 1 M NH_4OH	500
W	WCl_5	EtOH	300	1 M NH_4OH	500
Ir	$IrCl_3{\cdot}xH_2O$	H_2O	300	DMSO	500
Pt	$H_2PtCl_6{\cdot}6H_2O$	H_2O	300	DMSO or 1 M NH_4Cl	500

TiO_2 and Al_2O_3 substrates

Carrier	Metal precursor	Dispersion solvent	T_1 (°C)	Washing solvent	T_2 (°C)
TiO_2	$H_2PtCl_6{\cdot}6H_2O$	H_2O	300	DMSO or 1 M NH_4Cl	500
Al_2O_3	$H_2PtCl_6{\cdot}6H_2O$	H_2O	300	DMSO or 1 M NH_4Cl	500